Aerospace Science and Technology 130 (2022) 107904

Contents lists available at ScienceDirect

Aerospace Science and Technology

www.elsevier.com/locate/aescte

Effect of combustion mode on thrust performance in a symmetrical tandem-cavity scramjet combustor

Mingjiang Liu [a], Mingbo Sun [a,*], Guoyan Zhao [a,*], Yu Meng [b,c], Yuhui Huang [d], Guangwei Ma [a], Hongbo Wang [a]

[a] Science and Technology on Scramjet Laboratory, National University of Defense Technology, Changsha, Hunan 410073, China
[b] School of Aeronautics and Astronautics, Shanghai Jiao Tong University, Shanghai 200240, China
[c] Institute of Mechanics CAS, Beijing 100190, China
[d] Equipment Project Management Center, Equipment Development Department, Beijing 100089, China

ARTICLE INFO

Article history:
Received 13 January 2022
Received in revised form 31 July 2022
Accepted 22 September 2022
Available online 4 October 2022
Communicated by Bing Wang

Keywords:
Tandem-cavity
Scramjet combustor
Combustion mode
Thrust performance

ABSTRACT

To investigate the relationship between the thrust performance and combustion mode in a scramjet combustor, the acceleration process of a symmetrical tandem-cavity combustor is numerically investigated based on previous experiments. The numerical results are essentially in agreement with the experimental results through high-speed photography and wall pressure comparisons, which verifies the reliability of the numerical method. Then, three groups of simulations with different equivalent ratios are designed under the condition of inlet flow Mach numbers 2.4, 2.5, 2.6, 2.7, and 2.9. Complete combustion efficiency and specific section thrust are defined to measure the combustion efficiency of kerosene and thrust performance. Four combustion modes are defined and observed in simulations, i.e. strong ram mode, weak ram mode, dual-mode ram mode, and scram mode. The simulation results show that the combustion modes in the former and the later cavities for this tandem-cavity scramjet combustor are related to each other. Combustion modes have a significant impact on the thrust performance of the combustor and the specific section thrust mutation is caused by mode transition. Under different inlet Mach numbers, appropriate equivalent ratio settings can improve thrust performance for this tandem-cavity supersonic combustor. Two ideal combustion modes realized by different injection schemes are proposed for better thrust performance of symmetrical tandem-cavity supersonic combustor.

1. Introduction

For hypersonic airplanes, dual-mode scramjet is a promising choice [1,2] to work over a wide Mach number range with a simple structure [3]. However, unsteady combustion is a very common phenomenon [4,5] which brings trouble to the control of scramjet [6]. Beside this, proper combustion mode is also critical to maintaining the superior performance of the scramjet combustor during flight. The thrust performance mutation of dual-mode scramjet which is unfavorable for thrust control is inevitable during acceleration because of mode transition.

Previous studies have shown that combustion mode depends on the inflow condition [7–9], fuel scheme [10–13], and combustor design [14–16]. The influence of most adjustable parameters on combustion mode has been widely recognized. Li et al. [8,9] studied the processes of mode transition of the combustor under different total temperatures (T_t) and total pressures (P_t). The lower the total temperature of the incoming flow is, the more easily the shock train is to disturb the upstream of the isolator. The more backward position of the choked thermal throat is, and the closer the combustion tends to the ram mode [8]. The dimensionless peak pressure of the combustor when mode transition occurred were 0.25, 0.41, and 0.5, and did not change with the change of the total pressure of the inflow [9]. Cao [14] studied the effects of geometry, heat release distribution, wall temperature, wall friction, and incoming flow components on the combustion mode transition boundary. The results show that: increasing of combustion chamber area expansion rate, reducing the heat release rate of the combustion chamber, the more water molecules in the incoming air, the lower the wall temperature of the combustion chamber, the smaller the friction of the combustion chamber wall, the engine is easier to work in scram mode. Conversely, the engine is easier to work in ram mode. Zhang et al. [17] developed a Laval nozzle with an alterable throat area to change the incoming flow Mach number in the isolator entrance, and a ram-scram transition had taken

* Corresponding authors.
E-mail addresses: sunmingbo@nudt.edu.cn (M. Sun), zhaoguoyan09@nudt.edu.cn (G. Zhao).

https://doi.org/10.1016/j.ast.2022.107904
1270-9638/

Nomenclature

T_t	Total temperature	ER_1, ER_2	Equivalence ratio of jet1,jet2
P_t	Total pressure	η	Complete combustion efficiency
Y_{O_2}, Y_{H_2O}, Y_{N_2}	Mass fraction of O_2, H_2O, N_2	$F_e/\dot{m}_0$	Specific section thrust

place when the incoming flow Mach number variation. In summary, heat release and gas expansion during combustion are the most important factors to affect combustion mode, the combustion tends to be ram mode when heat release and gas expansion are promoted.

For combustion mode classification, there are several ways to classify combustion mode [18]. Zhang et al. [19] classified the combustion modes based on the flow field structure, namely scramjet mode, weak ramjet mode, and strong ramjet mode. The scramjet mode operation is characterized by supersonic combustion flow with no large-scale flow separation and combustion-induced pressure rise downstream of the primary fuel injection site. In contrast, the ramjet mode operation is characterized by subsonic combustion flow with large-scale flow separation and combustion-induced pressure upstream of the primary fuel injection site [20]. Then, Zhang et al. [19] proposed a simple judgment method for the combustion modes monitoring according to monitor pressure. Xiao et al. [21] established a quantificational distinguish criterion of combustion mode using wall pressure p_0 of outlet and p_i of the inlet for isolator. The combustor works in scram-mode when the pressure ratio is less than 1.5, while it is in ram-mode when the value of p_0/p_i is over 1.5. Tian et al. [22] associated the combustion mode with flame stabilization mode. Flame stabilization mode of scramjet mode was cavity shear layer stabilized combustion, and that of ramjet mode was combined cavity shear layer/recirculation stabilized combustion. Similarly, Cai et al. [10] obtained two combustion modes named the cavity shear-layer stabilized mode and the combined cavity shear-layer/recirculation stabilized mode with different fuel equivalence ratios. Masumoto et al. [23] obtained four combustion modes in a directly connected wind tunnel, namely non-ignition, weak combustion (reaction was active in the mixing layer between the airflow and fuel jet), supersonic combustion, and dual-mode combustion. By the comparison between schlieren photographs with different equivalence ratios, Zhang et al. [12] observed the intense oblique shock wave generated in the pure scram mode disappears, and the bifurcated shock wave occurs with the increase of the equivalence ratio. Then, the shock waves are pushed into the upstream isolator in the dual-mode ram mode.

After analyzing different combustion mode classifications, Huang et al. [24] believe that the weak combustion mode corresponds to the scram mode, while the intensive one is the ram mode, and the subsonic zone appears in the combustor chamber [12]. Then, the supersonic combustion mode and the dual-mode supersonic combustion mode defined by Tian et al. [22] belong to the weak combustion mode, and the dual-mode subsonic combustion mode and the subsonic combustion mode belong to the intensive combustion mode.

Many studies [25–27] have shown that the combustion mode has a significant impact on the performance of the combustor. Under the assumption of inviscid flow, Yang et al. [28] developed a series of equations to identify combustion mode transition analytically and hold the view that combustion mode transition is a nonlinear and unstable process. Zhang [29] used a direct-connect supersonic combustion test facility to study the influence of the historical adjustment direction of the equivalent ratio on the thrust of the supersonic combustor. Compared with the historical equivalent ratio decrease path, the thrust mutation on the equivalent ratio increase path is greater. Cao et al. [27] analyzed the combustion mode transition with the thermodynamic cycle analysis method and found that the Ram-mode cycle enjoys a significant specific thrust advantage over the Scram-mode cycle when the free stream Mach number is less than 6. But the result is the opposite when the free stream Mach number is greater than 7. Turner and Smart [11] obtained two combustion modes by increasing the equivalence ratio, namely “supersonic” combustion and “separated” combustion. Further, the combustion in the separated mode proved to generate higher thrust levels than the supersonic combustion mode, even at the relatively high Mach number of eight. Numerical demonstration by Kouchi et al. [25] indicated that the installation of auxiliary igniters on the sidewalls improved ignition capability and delivered higher thrust at a low equivalence ratio. The auxiliary igniters prevented the sudden change in the thrust that was unfavorable for engine control. Meng et al. [30] experimented to explore the acceleration process of the scramjet combustion chamber and found that when the mode transition occurs upstream, the downstream ramjet mode can eliminate the instability, which means that the overall thrust performance of the engine is stable. When the transition mode occurs downstream, the thrust fluctuates, indicating that the mode transition is an unstable process.

The dual-mode scramjet is designed to work over a wide Mach number range, while most previous studies were in a specific condition with a fixed Mach number. Meng et al. [30] provide an experimental technique in which the flow Mach number can be changed continuously. The present study simulated five typical working conditions during the acceleration process of reference [30] by three-dimensional compressible Reynolds-Averaged Navier-Stokes (RANS) simulation to further explore the effect of combustion mode on thrust performance. The numerical method in this paper has been fully verified by comparisons between numerical results and experimental high-speed photography and wall pressure. This study focuses on the overall performance and one-dimensional information of scramjet combustor. Consequently, the quasi-steady RANS simulation results can provide enough information. Different from reference [30], all combustion modes of cavities in tandem are analyzed and more detailed flow field structures are displayed. The flow field characteristics of different combustion modes are analyzed in detail. Different equivalent ratio allocations are designed because it is a key setting for the combustion modes of this scramjet combustor with tandem injections. For this scramjet combustor with tandem cavities and injections, the combustion efficiencies of kerosene are measured by the complete combustion efficiency of injections (η) and the complete combustion efficiency (η_t). Combustion efficiency is regarded as the link between combustion mode and thrust performance, and the relationship between mode transition and thrust variation is revealed in this study.

2. Experimental description and numerical method

2.1. Experimental setup and grid simplification

Experiments were conducted using the variable Mach number direct-connect supersonic combustor of Institute of Mechanics Chinese Academy of Sciences [30]. The heater combusts air, hydrogen, and oxygen, and the oxygen mole fraction is 21% after combustion. The Mach number at the nozzle can be varied from Ma 1.7 to

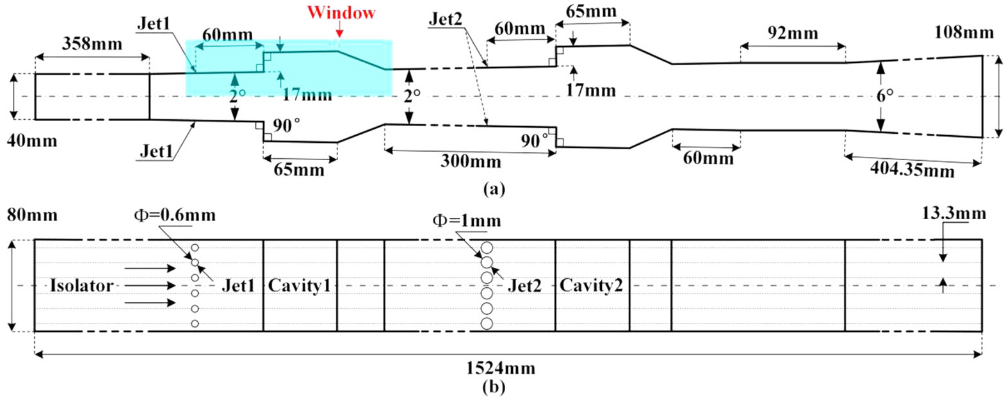

Fig. 1. Front (a) and top (b) view of scramjet combustor.

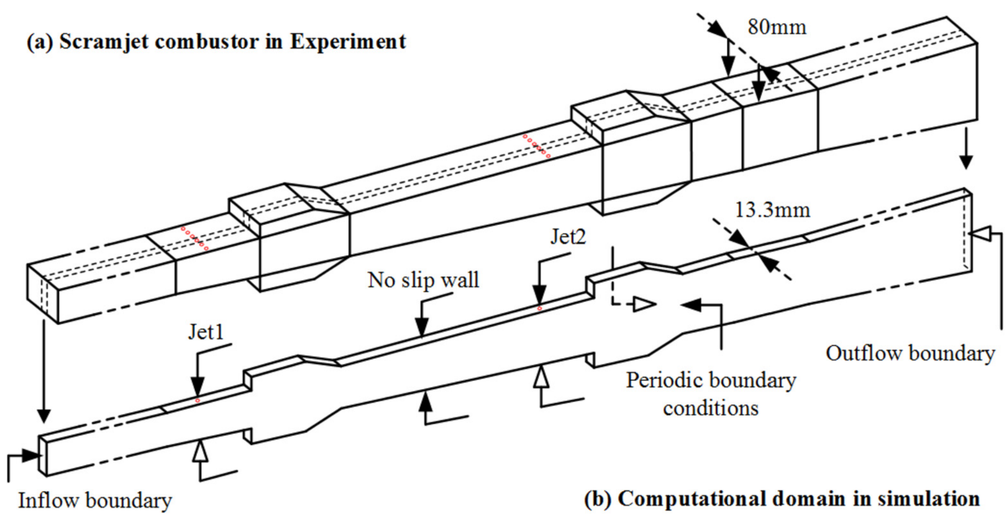

Fig. 2. Schematics diagram of scramjet combustor (a) and computational domain (b).

Table 1
Isolator inlet boundary conditions.

Condition (Cases)	*Ma*	T_t (K)	P_t (MPa)	Y_{O2} (%)	Y_{H2O} (%)	Y_{N2} (%)
F1(A1,B1,C1)	2.4	1228	1.47	24.37	8.69	66.94
F2(A2,B2)	2.5	1363	1.57	24.59	10.08	65.33
F3(A3,B3,C2)	2.6	1493	1.55	24.78	11.45	63.78
F4(A4,B4)	2.7	1591	1.66	24.87	12.50	62.63
F5(A5,B5,C3)	2.9	1686	1.98	25.01	13.57	61.43

3.2. The inlet total temperature and mass flow rate are changed by varying the hydrogen, oxygen, and airflow rate. The typical isolator inlet boundary conditions as a reference in the simulation are shown in Table 1.

The combustor is symmetrical and has a rectangular cross-section. The size of the supersonic combustor in experiments is shown in Fig. 1. There are two symmetrically distributed cavities for flame stabilization as shown in Fig. 1 (a). CH* observation window is performed only in the first cavity. The fuel is room-temperature kerosene RP3, the jet is vertically sprayed. Two groups of symmetrically distributed fuel jets are both 60 mm upstream of the cavity. The fuel jet diameter of the first group is 0.6 mm while the second is 1 mm, and the spacing between adjacent jets is 13.3 mm. The first groups of cavities and fuel jets are marked as Cavity1 and Jet1, and the second groups are marked as Cavity2 and Jet2. The fuel was injected into the combustor at sonic velocity. The injection pressures were given according to the mass flow rates of the isolator inlet (F1∼F5 in Table 1) and the equivalence ratios of Jet1 and Jet2. More details are seen in reference [30].

To reduce the calculation time, 1/6 of the scramjet combustor is selected as the computational domain. Fig. 2 shows the selection of the computational domain. A no-slip, no-penetration, and adiabatic condition is set at the upper and lower wall. Both sides of the computational domain are set as periodic boundary conditions as shown in Fig. 2(b). Inflow and outflow boundary conditions are imposed at the entrance and exit.

2.2. Governing equations and numerical setups

The RANS simulation has been widely used in engineering applications and academic research because it can capture the main characteristics of the flow field with small calculation efforts. For the combustion process, the density changes with the heat release process, so the Favre-averaged method is convenient in simulation. The governing equations of the compressible Navier-Stokes equations together with the species transport equations [31] can be written as below

$$\frac{\partial \bar{\rho}}{\partial t}+\frac{\partial\left(\bar{\rho}\tilde{u}_i\right)}{\partial x_i}=0 \tag{1}$$

$$\frac{\partial \bar{\rho}\tilde{u}_i}{\partial t}+\frac{\partial\left(\bar{\rho}\tilde{u}_i\tilde{u}_j\right)}{\partial x_j}=-\frac{\partial \bar{p}}{\partial x_i}+\frac{\partial \bar{\pi}_{ij}}{\partial x_j}+\frac{\partial \bar{\tau}_{ij}}{\partial x_j} \tag{2}$$

$$\frac{\partial\left(\bar{\rho}\tilde{E}\right)}{\partial t}+\frac{\partial\left(\bar{\rho}\tilde{h}\tilde{u}_j\right)}{\partial x_j}=\frac{\partial}{\partial x_j}\left(\tilde{u}_i(\bar{\pi}_{ij}+\tau_{ij})-Q_j\right) \tag{3}$$

$$\frac{\partial\left(\bar{\rho}\tilde{Y}_\alpha\right)}{\partial t}+\frac{\partial\left(\bar{\rho}\tilde{Y}_\alpha\tilde{u}_j\right)}{\partial x_j}=\frac{\partial}{\partial x_j}\left(D_\alpha\frac{\partial\tilde{Y}_\alpha}{\partial x_j}\right)-\frac{\partial M_{j\alpha}}{\partial x_j}+\tilde{\dot{\omega}}_\alpha \tag{4}$$

where

$$\pi_{ij}=\mu(\tilde{T})\left(\frac{\partial\tilde{u}_i}{\partial x_j}+\frac{\partial\tilde{u}_j}{\partial x_i}-\frac{2}{3}\frac{\partial\tilde{u}_k}{\partial x_k}\delta_{ij}\right) \tag{5}$$

$$\tau_{ij}=\bar{\rho}\nu_t\left(\frac{\partial\tilde{u}_i}{\partial x_j}+\frac{\partial\tilde{u}_j}{\partial x_i}-\frac{2}{3}\frac{\partial\tilde{u}_k}{\partial x_k}\delta_{ij}\right) \tag{6}$$

$$Q_j=-\left(\kappa(\tilde{T})+\bar{\rho}c_p\frac{\nu_t}{Pr_t}\right)\frac{\partial\tilde{T}}{\partial x_j}-\bar{\rho}\frac{\nu_t}{Sc_t}\sum_s^N\tilde{h}_s\frac{\partial\tilde{Y}_s}{\partial x_j} \tag{7}$$

$$Ma_{j\alpha}=-\bar{\rho}\frac{\nu_t}{Sc_t}\frac{\partial\tilde{Y}_\alpha}{\partial x_j} \tag{8}$$

Here, $\mu(\tilde{T})$ and ν_t are molecular and eddy viscosities, respectively, $\kappa(\tilde{T})$ heat conductivity, '–' and '∼' the temporal averaging for RANS and the Favre filtering, respectively, and Favre filtering is defined by

$$\tilde{\phi}=\frac{\int_0^{\Delta t}\rho(t)\phi(t)dt}{\int_0^{\Delta t}\rho(t)dt}=\frac{\overline{\rho\phi}}{\bar{\rho}} \tag{9}$$

The in-house code employed with the finite volume method had shown excellent performance in solving the above equations [32]. The SST k-ω turbulent model [33] is employed to calculate the turbulent viscosity for its good performance in the supersonic combustion process. 4 steps 2nd order Runge-Kutta method [34] is applied for time advancement. The Courant-Friedrichs-Lewy (CFL) number, which controls the speed of the calculation, is set to 0.1 firstly and improved to 0.2 to avoid numerical divergence. The flow field is considered reaching the quasi-steady state when the mass flow rate of the inflow and fuels jet approximately equals that of the outflow with an error below 1%.

The flamelet-progress variable (FPV) combustion model was implanted into the code to calculate the supersonic turbulent combustion which has been verified previously [35–38] since it has a low computational cost. Gaseous n-dodecane was injected into the combustor as a substitute for kerosene and the equivalence ratios in simulations were consistent with that in the experiments. The combustion reaction mechanism [39] of n-dodecane which contains 369 species and 2691 elementary reactions was used to simulate the kerosene combustion process.

The steady flamelet equations were solved by the FlameMaster V3.3.9 software package [40]. The laminar flamelet databases were generated with the assumption that the Lewis number of all components is 1. The reference pressure is 3atm, and the temperatures of oxidant and fuel were set as 1000 K and 300 K respectively. 59 laminar flamelet databases were generated, and turbulent flamelet databases [41,42] were obtained by averaging ensemble employed with the presumed-PDF method [43] based on laminar flamelet databases.

2.3. Numerical method verification

To verify the numerical results, the pressure ratio of experiment A3 ($Ma = 2.6$) is compared with the numerical result. Simulations based on coarse (8.134 million), medium (12.39 million), and refined (18.16 million) grids are conducted and compared with the pressure ratio as shown in Fig. 3. The wall pressures of the medium and refined grids are almost similar to each other while the result of the coarse grid is greatly deviating. The coarse grid cannot calculate the wall pressure at the cavities accurately. To ensure sufficient accuracy in simulation, the refined grid is selected

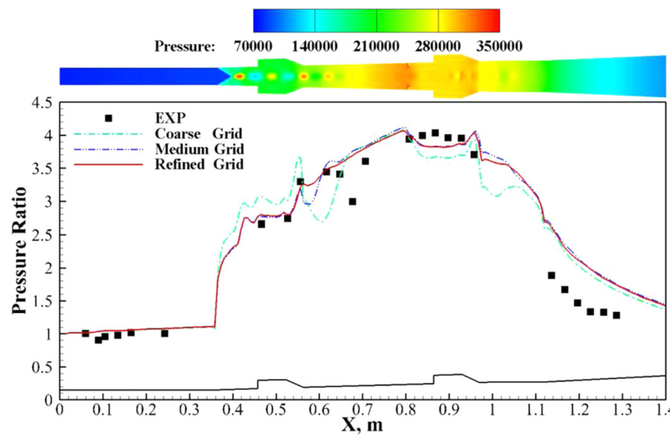

Fig. 3. Comparison of wall pressure ratios between numerical and experimental results along the centerline on the upper wall of the scramjet [30].

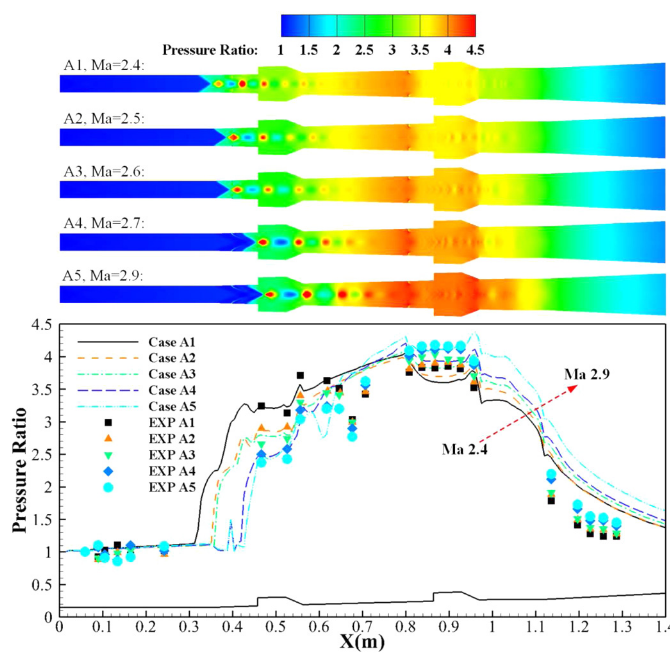

Fig. 4. Comparison of wall pressure ratios between experimental (left) and numerical (right) along combustor path with different inlet flow Mach number.

to perform the simulation. All grids are refined near the wall and injection orifices. The inflow condition was changed continuously in the experiment [30], therefore it is difficult to restore the real inflow condition at $Ma = 2.6$. The experimental data in Fig. 3 is a reference for case A3.

To verify the numerical results under different inlet conditions, the wall pressure of five cases (A1∼A5) was compared with the pressure during acceleration in Fig. 4. It can be found that the significant pressure rise position moves backward and the pressure ratio at Jet1 gets lower with the increase of Mach number, and the experimental data also show the same law. The pressure ratio peaks in Cavity2 and drops in the expansion section for both simulation and experiment. After Jet2, the higher the Mach number, the higher the pressure ratio. In the expansion section, the pressure of the simulation is higher than that in the experiment. However, since the combustion mode in cavities is not affected, the difference does not affect the reliability of this study. In general, the simulation and experiment show the same pressure variation law

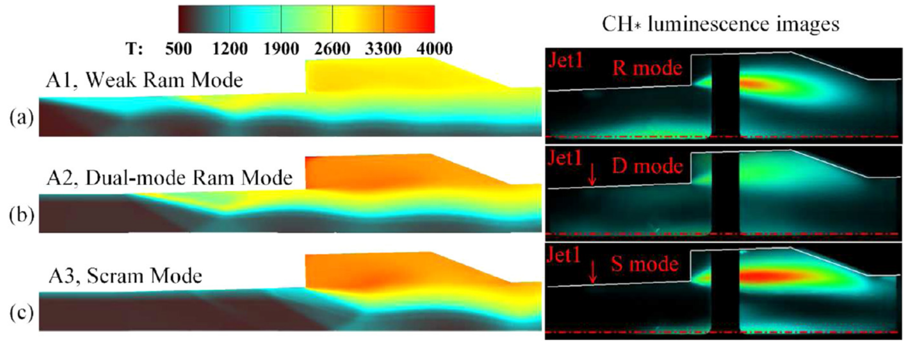

Fig. 5. Numerical temperature contours and time-averaged CH* luminescence images of three different combustion modes.

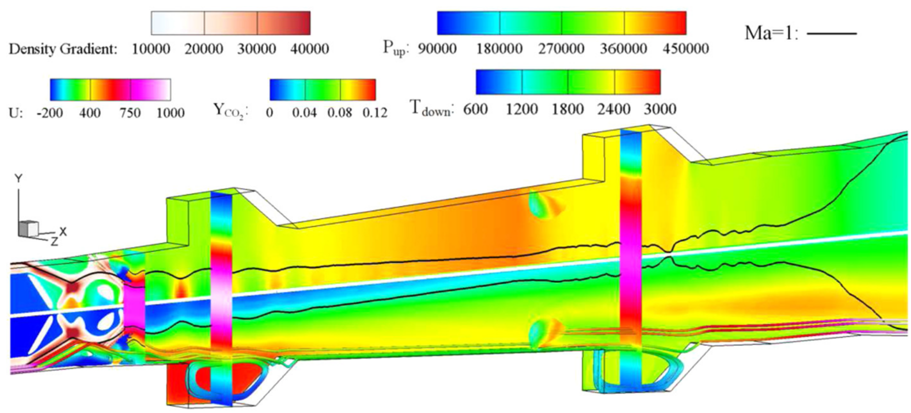

Fig. 6. The flow field of A1. The Z=0 plane is lined by $Ma = 1$ and contoured by pressure (upper) and temperature (lower). The stream rods and X planes are colored by velocity in the X-direction. The iso-surfaces ($Y_{C_{12}H_{26}} = 0.018$) are contoured by Y_{CO_2}.

during acceleration, and the wall pressure comparison also shows that simulation can predict the flow field precisely.

Fig. 5 shows three combustion modes observed in simulations and experiments. Combustion mode is the central issue in this article. Different combustion modes are important objects that need to be simulated in this study. The combustion region of the weak ram mode (A1) is smaller than the dual-mode ram mode (A3) because the total temperature of A1 ($Ma = 2.4$) is lower than A3 ($Ma = 2.6$). For scram mode, the combustion region mainly exists in the cavity and its shape is affected by the interaction of oblique shock waves. There are some differences between the numerical results and CH* luminescence images. Flame exists in the center of the combustor due to various small structural defects in the experiment which changed the structure of the combustion flow field. In both experiments and simulations, the size of the combustion region is closely related to the combustion mode. The flame region becomes smaller and moves downstream when combustion mode is transformed from weak ram mode to scram mode.

On the other hand, the inlet and injection conditions in the experiments are constantly changing. While in the simulations, some specific moments in the experiment are selected and restored by RANS simulation method. In addition, the transient CH* luminescence images are different from the temperature contours in simulations.

3. Analysis of combustion flow field and thrust performance of the dual-mode scramjet combustor

In section 2.3, the reliability of the numerical method in section 2.2 has been verified, and the following simulations are based on the same numerical method. In this section, three groups (A, B, and C) were designed to study the relationship between combustion mode and thrust performance for the multi-cavity scramjet combustor. In section 3.1, group A with a fixed equivalent ratio was firstly simulated based on full verification. Group B with a continuously changing equivalent ratio of Jet2 was designed. Group A and B were analyzed to research the mode transition and the change of thrust performance during acceleration. In section 3.2, group C with an adjusted equivalent ratio allocation of Jet1 and Jet2 was compared with groups A and B to study the effect of equivalent ratio on combustion mode and thrust performance under different inflow conditions.

3.1. Mode transition and thrust change during acceleration

For this multi-cavity supersonic combustor, the combustion flow field presents a similar structure during acceleration. Fig. 6 displays the typical flow field structure by taking A1 as an example. The inlet Mach number of A1 is 2.4 and the flow field structure is symmetrically distributed. The bow shock waves are formed in front of the iso-surface of the fuel mass fraction. Flow separation occurs near the upstream wall and a stable recirculation zone is formed upstream of Jet1 which helps fuel mixing and stabilize the flame. Strong oblique shock waves are formed upstream of cavities and intersect in the center of the combustor. The shock train generated by the intersection of oblique shock waves exists up to the downstream of Cavity1 and produces discontinuous high-pressure zones in the center of the combustor. The pressure in the combustor peaks near Cavity2 and falls downstream of Cavity2. The combustion mode in Cavity1 is weak ram mode and heat release exists upstream of Jet1. It can be seen in the temperature contour that the combustion in Cavity1 is the cavity shear-layer stabilized combustion mode while the combustion in Cavity2 is jet-wake stabilized combustion mode. Three main recirculation regions can be seen in cavities and upstream of Jet1 from Fig. 6, and a small recirculation region exists downstream of Jet1. The fuel iso-surfaces

Table 2
Four combustion modes classification for supersonic combustor with tandem cavities.

Combustion zone	Major factor		Combustion mode	Shock train position and Significant pressure rise position	1-D Mach number
Cavity1	Ma	Low ↓ High	Weak ram mode Dual-mode ram mode Scram mode	Upstream of Jet1 Near Jet1 Downstream of Jet1	Greater than 1
Cavity2	ER_2	High ↑ Low	Strong ram mode Weak ram mode Dual-mode ram mode	None Upstream of Jet2 Near Jet2	Less than 1 Greater than 1

Table 3
Simulation parameters for fixed equivalence ratio (A).

Case	Ma	T_t (K)	P_t (MPa)	ER_1	ER_2
A1∼A5	2.4∼2.9	1228∼1686	1.47∼1.98	0.2	0.65

are contoured by the mass fraction of carbon dioxide. It is clear to see that the combustion mainly occurs near the wall for Jet1 while combustion mainly occurs in the jet wake of Jet2. Sonic lines at Cavity1 are affected by shock trains and a thermodynamic throat is formed at Cavity2 which is beneficial for the combustor to work in strong ram mode.

Four combustion modes were observed and defined with different characteristics as shown in Table 2. For group A, the combustion mode at Cavity1 transitions from ram mode to scram mode, and the combustion mode at Cavity2 is strong ram mode with the increase of Mach number. For group B, the combustion mode at Cavity1 transitions from ram mode to scram mode, and the combustion mode at Cavity2 transitions from strong ram mode to dual-mode ram mode with the increase of Mach number. In this section, such phenomena during acceleration will be described and analyzed in detail.

3.1.1. Analysis of combustion flow fields and combustion modes with a fixed equivalence ratio

Thrust change is the most concerned question for dual-mode scramjet engines, while it is inevitable because of mode transition during acceleration. Group A with a fixed equivalence ratio during acceleration is simulated. Table 3 shows the simulation parameters and injection schemes during acceleration, where T_t is the total temperature; P_t is the total pressure; ER_1 and ER_2 are the equivalent ratios of the former and the later fuel injections, respectively.

Fig. 7 shows the changes of temperature contours, recirculation zones, and sonic lines when the Mach number increases from $Ma = 2.4$ to $Ma = 2.9$. Mass averaged one-dimensional Mach number distribution and wall pressure ratio along the combustor path of group A are also drawn in Fig. 8 and Fig. 9. The inlet Mach number changes along the direction of the red arrow.

When the Mach number increases from 2.4 to 2.6, the recirculation zone upstream of Jet1 is compressed and the recirculation zone downstream of Jet1 plays a more significant role in fuel mixing and combustion. As shown in Fig. 8, the shock train moves back to the injection position which means the combustion mode in Cavity1 is dual-mode ram mode when $Ma = 2.5$, 2.6 according to the definition in Table 2. The shock train and significant pressure rise position continue to move backward with the increase of Mach number. The recirculation zone downstream of Jet1 disappears when the $Ma = 2.7$, then the recirculation zone in Cavity1 bulges, and a new flame stabilization and mixing mode is formed in Cavity1. By observing the relative position [20] of the combustion-induced pressure rise position and the site of Jet1 (Fig. 9), it can be found that the ram-to-scram mode transition occurs in Cavity1.

For Cavity2, the mass averaged one-dimensional Mach number is always less than 1 during acceleration as shown in Fig. 8.

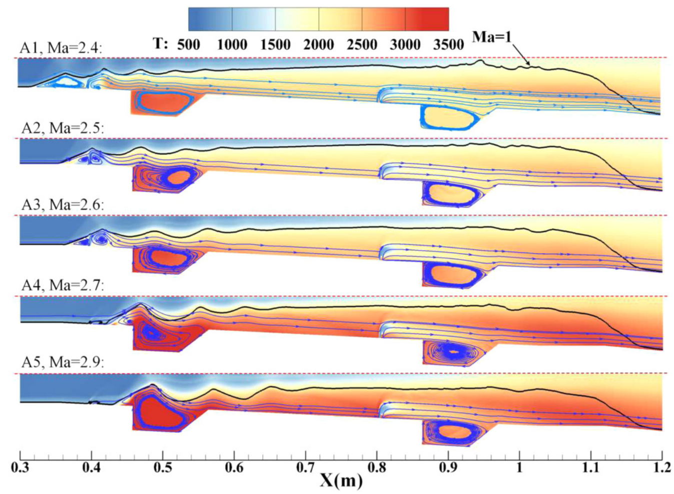

Fig. 7. Temperature contours and $Ma = 1$ lines in the center planes and streamlines in recirculation zones with different inlet flow Mach numbers for group A.

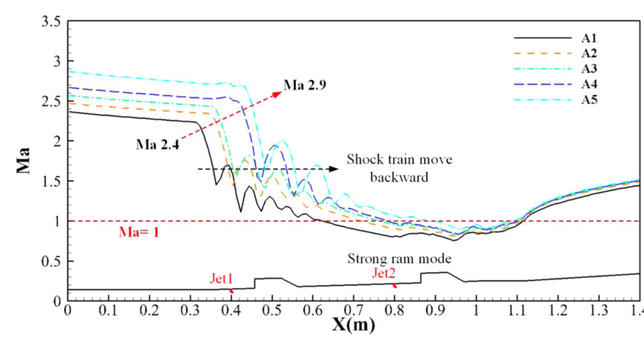

Fig. 8. Mach number distributions along combustor path with different inlet flow Mach numbers for group A.

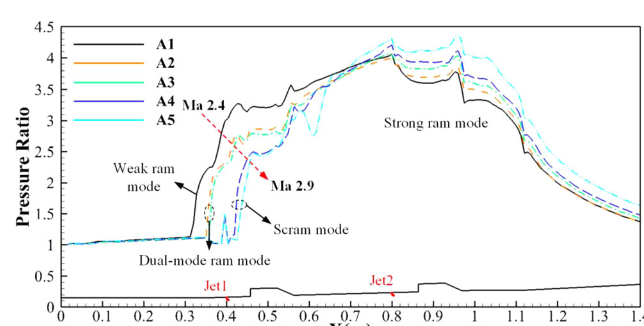

Fig. 9. Pressure ratios along combustor path with different inlet flow Mach numbers for group A.

The pressure ratio peaks in Cavity2 and shows a similar law with the previous study [9] (The higher the total pressure, the lower pressure ratio). The sonic line expands during acceleration which means the thermodynamic throat area becomes smaller. The flow

Table 4
Simulation parameters for continuously changing equivalence ratio of Jet2 (B).

Case	Ma	T_t (K)	P_t (MPa)	ER_1	ER_2
B1∼B5	2.4∼2.9	1228∼1686	1.47∼1.98	0.2	0.56, 0.53, 0.43, 0.36, 0.26

field structure in Cavity2 is unchanged and combustion remains strong ram mode during acceleration.

3.1.2. Analysis of combustion flow fields and combustion modes with a continuously changing equivalence ratio of Jet2

In this section, group B with the continuously changing equivalence ratio of Jet2 during acceleration is simulated. Table 3 shows the simulation parameters and injection schemes during acceleration, where T_t is the total temperature; P_t is the total pressure; ER_1 and ER_2 are the equivalent ratios of the former and the later fuel injections, respectively. (See Table 4.)

Fig. 10 shows the combustion flow field of group B. Mass averaged one-dimensional Mach number distribution and wall pressure ratio along the combustor path of group B are also drawn in Fig. 11 and Fig. 12.

When the Mach number increases from 2.4 to 2.7, the recirculation zone upstream of Jet1 is compressed and the recirculation zone downstream of Jet1 plays a more significant role in fuel mixing and combustion. The shock train and significant pressure rise position continue to move backward with the increase of Mach number. Different from group A, the recirculation zone downstream of Jet1 plays a significant role in fuel mixing, and the bulge of the recirculation zone in Cavity1 is not formed when Ma = 2.7. Meanwhile, the combustion-induced pressure rise site of B4 is upstream of Jet1 which means mode transition does not occur when Ma = 2.7. In addition, the phenomenon of sonic lines reattachment appears in group B, which means the bow shock wave in front of Jet2 will produce greater flow loss.

The equivalence ratio of Jet1 is not changed compared with group A while the mode transition in Cavity1 is different from group A. As shown in Fig. 12, the pressure of B4 and B5 at Cavity1 is higher than that of B3 which is different from group A. It is noticed that the mode transition in Cavity2 leads to the reduction of back pressure before Jet2 which is conducive to the heat release and gas expansion in Cavity1. Therefore, the combustion in Cavity1 tends to be ram mode when combustion mode in Cavity2 is weak ram mode. In summary, the combustion modes of the two cavities are not independent for the tandem-cavity combustor, and the combustion mode of Cavity1 is affected by the combustion mode of Cavity2.

For combustion in Cavity2, combustion mode is transformed from strong ram mode to weak ram mode when Ma = 2.6. As seen in Fig. 11 and Fig. 12, the mass averaged one-dimensional Mach number is higher than 1 (Fig. 11) and the pressure ratio decreases significantly upstream of Jet2 (Fig. 12) when $Ma > 2.6$. The shock train reappears in weak ram mode and moves backward with the increase of Mach number.

3.1.3. Analysis of combustion efficiency and specific section thrust

The combustion efficiencies of different combustion modes are worthy of attention for the thrust performance of scramjet combustors. The combustion efficiencies and the specific section thrusts of group A and B are both analyzed and compared in this section.

Pyrolysis of macromolecular hydrocarbons is inevitable under high total temperatures. The combustion efficiency defined by the mass flow rate of residual fuel is inapplicable to measure the performance of the combustion chamber because the kerosene combustion mechanism [39] used in this paper is a complex multi-step reaction. To analyze the combustion efficiency of kerosene in the

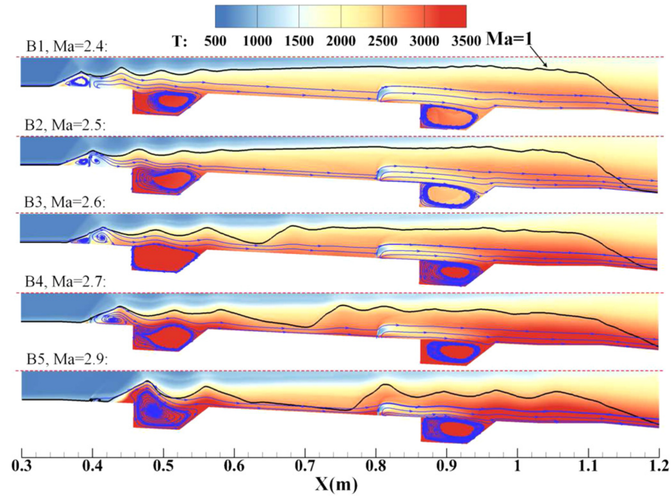

Fig. 10. Temperature contours and $Ma = 1$ lines in the center plane and streamlines in recirculation zones with different inlet flow Mach numbers for group B.

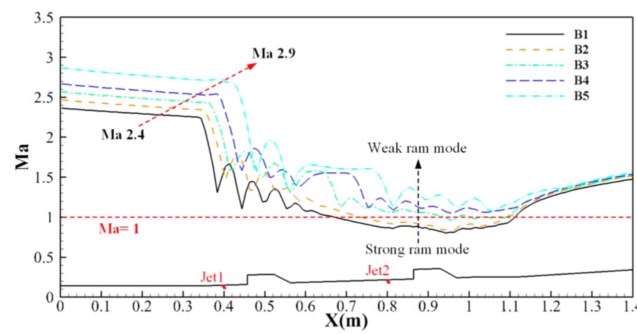

Fig. 11. Mach number distributions along combustor path with different inlet flow Mach numbers for group B.

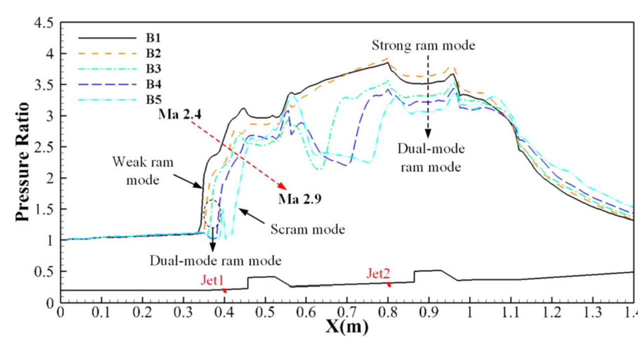

Fig. 12. Pressure ratios along combustor path with different inlet flow Mach numbers for group B.

scramjet combustor, the complete combustion efficiency is defined by complete combustion products.

$$\eta_{CO_2}(x) = \frac{\int_{A(x)} \rho Y_{CO_2} u dA}{k_{CO_2} \cdot \dot{m}_{fuel-jet}} \tag{10}$$

where k_{CO2} is the mass flow rate ratio of CO_2 to fuel jet after complete combustion, $k_{CO_2} = 3.106$ when the fuel is $C_{12}H_{26}$.

For the combustor with two injection positions, complete combustion efficiencies of Jet1 and Jet2 are calculated respectively.

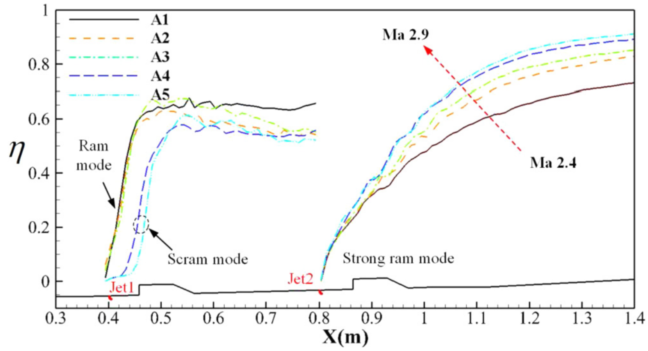

Fig. 13. Total combustion efficiencies of injections along combustor path with different inlet flow Mach numbers for group A.

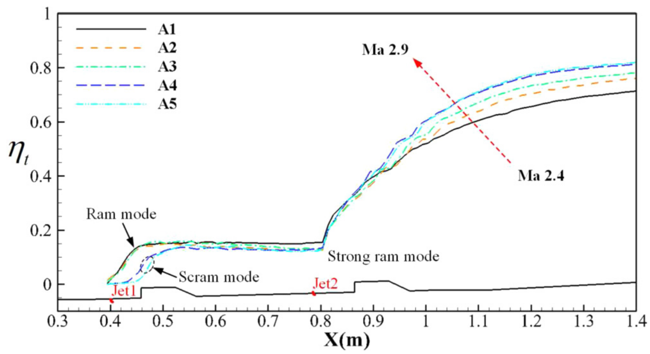

Fig. 14. Total combustion efficiencies along combustor path with different inlet flow Mach numbers for group A.

$$\eta_{Jet1}(x_{Jet1} < x_1 < x_{Jet2}) = \frac{\int_{A(x_1)} \rho Y_{CO_2} u dA}{k_{CO_2} \cdot \dot{m}_{fuel-Jet1}},$$
$$\eta_{Jet2}(x > x_{Jet2}) = \frac{\int_{A(x_2)} \rho Y_{CO_2} u dA - \int_{A(x_1)} \rho Y_{CO_2} u dA}{k_{CO_2} \cdot (\dot{m}_{fuel-Jet1} + \dot{m}_{fuel-Jet2})} \quad (11)$$

The complete combustion efficiency is also calculated to analyze the overall performance of the combustor.

$$\eta_t(x > x_{Jet1}) = \frac{\int_{A(x)} \rho Y_{CO_2} u dA}{k_{CO_2} \cdot (\dot{m}_{fuel-Jet1} + \dot{m}_{fuel-Jet2})} \quad (12)$$

Fig. 13 shows the complete combustion efficiencies of Jet1 and Jet2. It can be seen clearly that there are great differences between ram mode and scram mode. Ram mode has higher combustion efficiency than scram mode. There is an obvious mutation in combustion efficiency in the process of mode transition (from $Ma = 2.6$ to $Ma = 2.7$) as shown in Fig. 13. For combustion at Cavity2, the higher the Mach number, the higher the combustion efficiency. This phenomenon is considered as inflow with a higher Mach number has a lower mass flow rate. Fig. 15 and Fig. 16 show the complete combustion efficiencies of group B. The complete combustion efficiency of B5 is higher than 1 because some fuel burned incompletely in Cavity1 is burned completely in Cavity2. It is noticed that group B with decreased equivalent ratio has higher combustion efficiency than group A, and the improvement of combustion efficiency leads to the increase of temperature, as seen in Fig. 7 and Fig. 10.

The previous study [11] showed that the ram mode proved to generate higher thrust levels than the scram mode. To explore the change of thrust performance during acceleration, specific section thrust along the combustor path of groups A and B is calculated and shown in Fig. 17 and Fig. 18. The specific section thrust is suitable for evaluating the comprehensive efficiency of combustion and flow in the combustor. Its calculation formula is as follows:

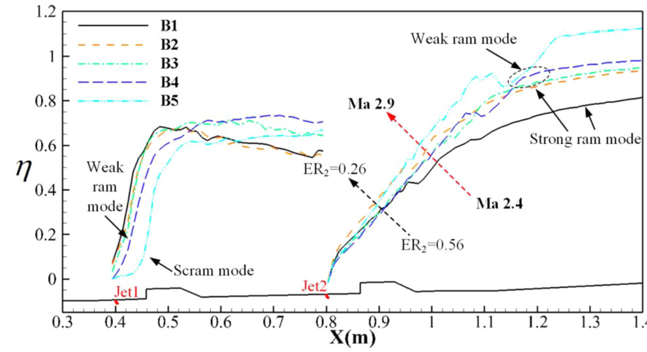

Fig. 15. Total combustion efficiencies of injections along combustor path with different inlet flow Mach numbers for group B.

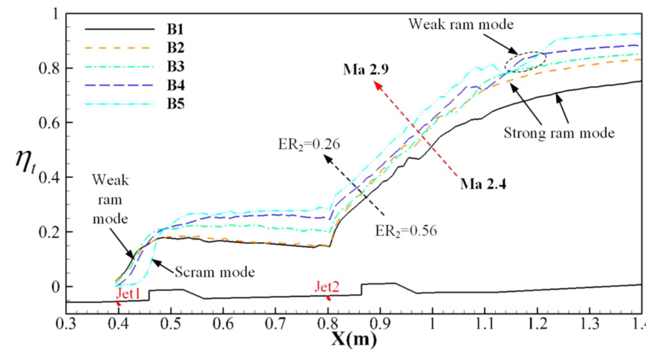

Fig. 16. Total combustion efficiencies along combustor path with different inlet flow Mach numbers for group B.

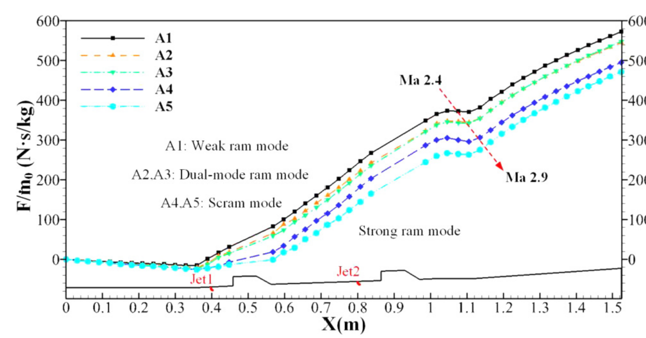

Fig. 17. Specific section thrust along combustor path with different inlet flow Mach numbers for group A.

$$\frac{F_e}{\dot{m}_0} = \frac{(\dot{m}_e V_e + P_e A_e) - (\dot{m}_0 V_0 + P_0 A_0)}{\dot{m}_0} \quad (13)$$

where F_e is inner thrust at section e, m_0 is the mass flow rate of the inlet.

Fig. 17 and Fig. 18 show the specific section thrust along the combustor path during acceleration. As we can see in Fig. 17, the specific section thrust goes through a decline process in the equivalent sections and rises rapidly in combustion zones and expansion sections. By observing the specific section thrust in Cavity1 of group A, the difference between A1∼A5 is mainly caused by the combustion mode in Cavity1. Combustion in ram mode can bring a faster specific section thrust increase than combustion in scram mode. For dual-mode ram mode, the specific section thrust curves of A2 and A3 along the combustor path are almost coincident. In general, the specific section thrust decreases with the increase of Mach number, and mutation occurs during mode transition.

The specific section thrust along the combustor path with a continuously changing equivalence ratio is shown in Fig. 18. Compared with the specific section thrust of group A, the specific

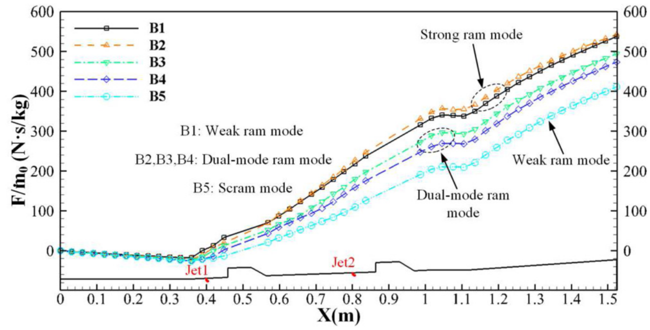

Fig. 18. Specific section thrust along combustor path with different inlet flow Mach numbers for group B.

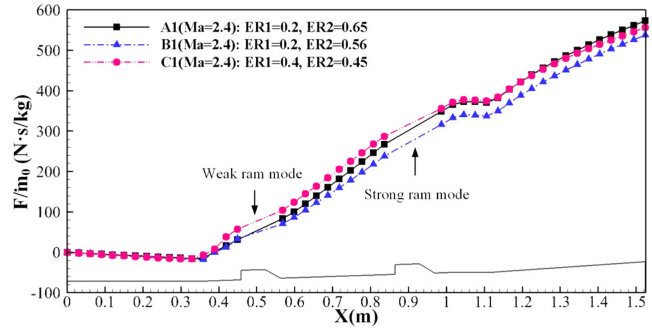

Fig. 20. Specific section thrust along combustor path with different equivalent ratios for $Ma = 2.4$.

Table 5
Simulation parameters for adjusted equivalent ratio allocation.

Case	Ma	T_t (K)	P_t (MPa)	ER_1	ER_2
C1	2.4	1228	1.47		
C2	2.6	1493	1.55	0.4	0.45
C3	2.9	1686	1.98		

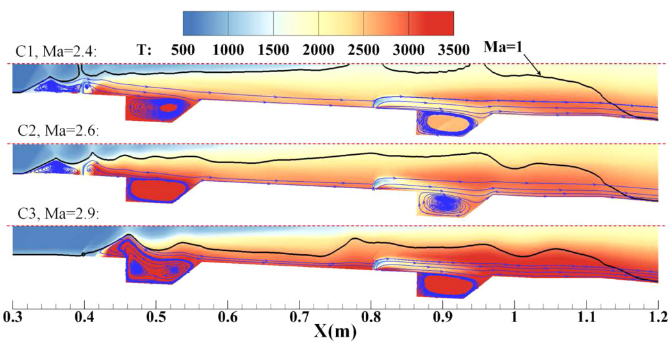

Fig. 19. Temperature contours and $Ma = 1$ lines in the center planes and streamlines in recirculation zones with different equivalent ratios for group C.

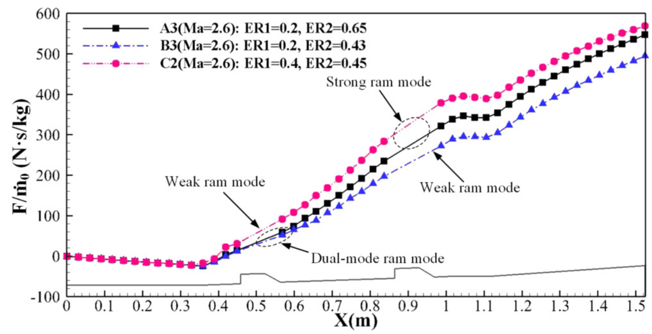

Fig. 21. Specific section thrust along combustor path with different equivalent ratios for $Ma = 2.6$.

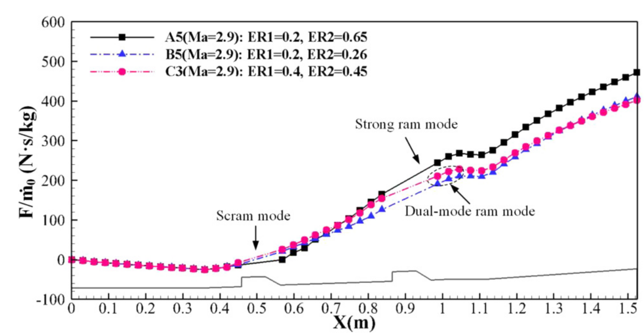

Fig. 22. Specific section thrust along combustor path with different equivalent ratios for $Ma = 2.9$.

section thrust of group B decreases when the equivalence ratio decreases. While the specific section thrust of B2 ($Ma = 2.5$) is also almost unchanged, the combustion modes of Cavity1 and Cavity2 do not change when the equivalence ratio is decreased. The reason for this phenomenon is that the reducing equivalent ratio of Jet2 improves the combustion efficiency as shown in Fig. 14 and Fig. 16. By analyzing the combustion modes and specific section thrust in Fig. 17 and Fig. 18, it is easy to find that the more variations of combustion mode, the greater change of specific section thrust.

In summary, the specific section thrust is sensitive to the combustion mode. The specific section thrust changes very little when mode transition does not occur, and the thrust mutation is always accompanied by mode transition.

3.2. Effect of equivalent ratio allocation on thrust performance

As an easily adjustable setting during acceleration, the effect of equivalent ratio allocation on thrust performance is concerned for this multi-cavity scramjet combustor. Table 5 shows the simulation parameters of group C with adjusted equivalent ratio allocation. The inlet conditions and total equivalent ratio of group C and group A are the same.

Fig. 7, Fig. 10, and Fig. 19 show the combustion flow field of A1, B1, and C1 ($Ma = 2.4$) with different equivalent ratios respectively. For case A1, the combustor works in weak ram mode at Cavity1 and strong ram mode at Cavity2. As shown in Fig. 19, the combustion mode changes a little while the sonic line changes significantly when the equivalent ratio is changed. When the equivalent ratio of Jet2 is adjusted to 0.56, the sonic line expands which means thermal throat area expansion. For C1 with an adjusted equivalent ratio allocation, thermal choke happens near two fuel injection positions. Through the comparison among A1, B1, and C1 in Fig. 20, it can be found that the adjusted equivalent ratio allocation (C1) cannot bring a higher specific section thrust when $Ma = 2.4$.

Fig. 7, Fig. 10, and Fig. 19 show the combustion flow field of A3, B3, and C2 ($Ma = 2.6$) with different equivalent ratios. The combustor works in strong ram mode in Cavity2, while the combustion mode in Cavity1 changes when the equivalent ratio allocation is adjusted. As shown in Fig. 19, when the equivalent ratio of Jet2 is adjusted to 0.43, the phenomenon of sonic lines reattachment appears between Cavity1 and Jet2. The combustion mode in Cavity1 of C2 is changed from dual-mode ram mode to weak ram mode after the equivalent ratio allocation is adjusted to ER_1=0.4 and $ER_2 = 0.45$. Meanwhile, the thermodynamic throat area of C2 is smaller than A3, although ER_2 of C2 is lower than A3.

Fig. 21 shows the specific section thrust along the combustor path of A3, B3, and C2 ($Ma = 2.6$). C2 with adjusted the equivalent

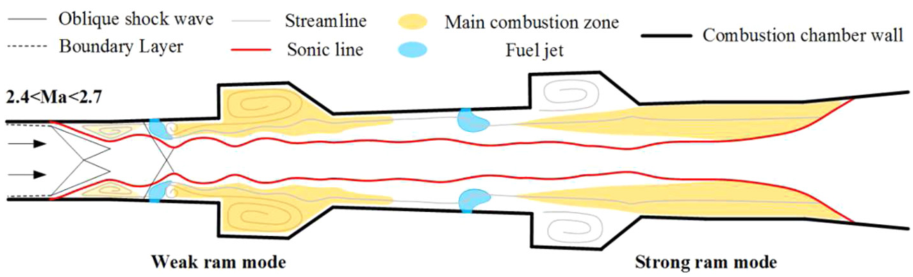

Fig. 23. Weak ram-strong ram mode when the inlet Mach number is less than 2.7.

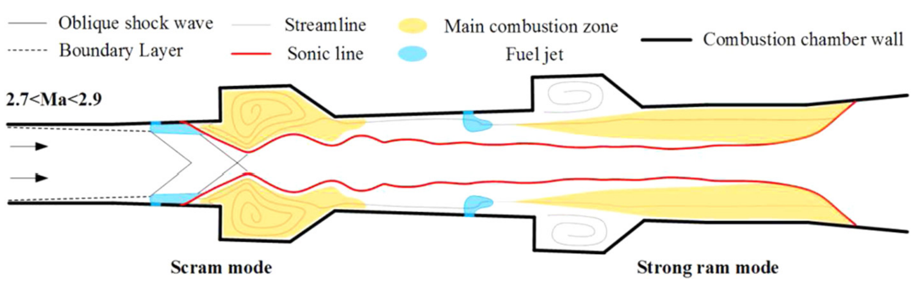

Fig. 24. Scram-strong ram mode when the inlet Mach number is greater than 2.7.

ratio allocation has a higher specific section thrust than A1. Similar to the previous conclusion, combustion mode is regarded as the most important factor affecting the thrust performance of scramjet combustor. Weak ram mode in Cavity1 can provide a large flow separation zone which contributes to strong ram mode forming in Cavity2. Therefore, adjusting the equivalent ratio allocation is a good choice to improve thrust performance when the inlet Mach number is 2.6.

Fig. 7, Fig. 10, and Fig. 19 show the combustion flow field of A5, B5, and C3 ($Ma = 2.9$) with different equivalent ratios. The combustor works in scram mode in Cavity1, while the combustion mode in Cavity2 changes when the equivalent ratio allocation is adjusted. As shown in Fig. 7, Fig. 10, and Fig. 19, when the equivalent ratio of Jet2 is decreased, the phenomenon of sonic lines reattachment appears between Cavity1 and Jet2. The combustion mode in Cavity1 is scram mode even though the equivalent ratio of Jet1 is $ER_1 = 0.4$. When $Ma = 2.9$, increasing the equivalent ratio of Jet1 cannot realize mode transition in Cavity1 to provide a large flow separation zone. The combustion mode of Cavity2 is mainly decided by the equivalent ratio of Jet2.

Fig. 22 shows the specific section thrust along the combustor path of A5, B5, and C3 ($Ma = 2.9$). A5 has a higher specific section thrust than B5 and C3. Combustion mode in Cavity1 is mainly decided by the inlet Mach number. Therefore, increasing the equivalent ratio of Jet2 is a suggested choice to improve thrust performance when the inlet Mach number is 2.9.

Based on the previous analysis in Sections 3.1 and 3.2, two ideal combustion modes at different Mach numbers are proposed for the symmetrical tandem-cavity scramjet combustor, named weak ram-strong ram mode for low Mach number and scram-strong ram mode for higher Mach number respectively. As shown in Fig. 23 and Fig. 24, the main difference between these two combustion modes is in the former cavity. It is noticed that the phenomenon of sonic lines reattachment does not appear in these two combustion modes, thermodynamic throat is formed at the later cavity. Previous results show that the combustor in these two combustion modes has a higher specific section thrust.

When the inlet Mach number is lower than 2.7, the combustion mode in Cavity1 is mainly decided by the equivalent ratio of Jet1. With the increase of inlet Mach number, increasing the equivalent ratio of Jet1 can help to stabilize the combustion in weak ram mode which is good for the thrust stability of the scramjet combustor. However, if the equivalent ratio of Jet1 is too high, the thermal choke will appear in Cavity1 which is unfavorable to the thrust generation of the scramjet combustor. Therefore, there should be an appropriate functional relationship between inlet Mach number and equivalence ratio allocation.

When the Mach number is higher than 2.7, the combustion mode in Cavity1 is mainly decided by the inlet Mach number. The combustion mode in Cavity1 is scram mode, and increasing the equivalent ratio of Jet1 has little effect on the mode transition in Cavity1. It is suggested to increase the equivalent ratio of Jet2 to make sure that the combustion mode in Cavity2 is strong ram mode which can help to maintain a better thrust performance.

4. Conclusion

The effect of the combustion mode on thrust performance during acceleration in a symmetrical tandem-cavity scramjet combustor is investigated numerically. The change characteristic of the combustion flow field in the combustor during acceleration is revealed, and it is found that the thrust performance of the combustor changes as combustion mode transition. Under different inlet Mach numbers, the effect of equivalent ratio allocation on the combustion modes of the tandem-cavity combustor is summarized. The relationship between combustion modes and thrust performance of tandem-cavity scramjet combustor is analyzed. The main conclusions are as follows:

For symmetrical tandem-cavity scramjet combustor, mode transition during the acceleration is characterized by the backward shift of shock train and significant pressure rise position. Strong ram mode, weak ram mode, dual-mode ram mode, and scram mode are observed and defined with different characteristics. The specific section thrust becomes higher when combustion mode transforms from scram mode to ram mode. While the thrust performance of the combustor will deteriorate when thermodynamic choking forms in the combustor. Mode transition among four combustion modes will cause thrust mutation of the scramjet combustor.

For scramjet combustors with tandem cavities, the combustion modes in the former and the later cavities are related to each other. If the combustion in the former cavity is ram mode, the combustion in the later cavity tends to be strong ram mode. It is believed that the ram mode in the former cavity can provide a large flow separation zone which contributes to the fuel mixing and combustion in the later cavity.

For scramjet combustors with tandem cavities and injections, the inlet Mach number is the most important factor affecting the combustion mode in the former cavity, and the equivalent ratio settings play a significant role in the mode transition of the later cavity. Under different inlet Mach numbers, appropriate equivalent ratio settings can improve the thrust performance of this tandem-cavity scramjet combustor. Two ideal combustion modes realized by different injection schemes are proposed for better thrust performance, named weak ram-strong ram mode for lower Mach number and scram-strong ram mode for higher Mach number respectively.

Declaration of competing interest

The authors declare that they have no known competing financial interests or personal relationships that could have appeared to influence the work reported in this paper.

Data availability

The data that has been used is confidential.

Acknowledgement

This work was supported by the National Natural Science Foundation of China [grant numbers 11925207, 12002381], the Scientific Research Plan of National University of Defense Technology in 2019 [grant number ZK19-02], and Science and Technology Foundation of State Key Laboratory under No. 6142703200311.

References

[1] K.R. Jackson, M.R. Gruber, S. Buccellato, Mach 6–8+ hydrocarbon-fueled scramjet flight experiment: the HIFiRE flight 2 project, J. Propuls. Power 31 (2015) 36–53.
[2] X.Y. Hao, J.T. Chang, W. Bao, Z. Zhang, A model of mode transition logic in dual-mode scramjet engines, Aerosp. Sci. Technol. 49 (2016) 173–184.
[3] X. Zhang, Combustion Flow Characteristics of Supersonic Combustion Mode Transitions and Hysteresis, University of Chinese Academy of Scienses, 2020.
[4] H.B. Wang, Z.G. Wang, M.B. Sun, N. Qin, Large-Eddy/Reynolds-averaged Navier-Stokes simulation of combustion oscillations in a cavity-based supersonic combustor, Int. J. Hydrog. Energy 38 (2013) 5918–5927.
[5] H.B. Wang, Z.G. Wang, M.B. Sun, Experimental study of oscillations in a scramjet combustor with cavity flameholders, Exp. Therm. Fluid Sci. 45 (2013) 259–263.
[6] M.B. Sun, H.B. Wang, Z. Cai, J.J. Zhu, Unsteady Supersonic Combustion, Springer, 2020.
[7] D.J. Micka, J.F. Driscoll, Combustion characteristics of a dual-mode scramjet combustor with cavity flameholder, Proc. Combust. Inst. 32 (2009) 2397–2404.
[8] J.P. Li, Z.L. Liao, G.Q. Jiao, W.Y. Song, The mode transition characteristics in a dual-mode combustor at different total temperatures, Energy 188 (2019) 116017.
[9] J.P. Li, G.Q. Jiao, J.Y. Luo, W.Y. Song, Effects of total pressure on mode transition in a dual-mode combustor, Acta Astronaut. 155 (2019) 55–62.
[10] Z. Cai, X.B. Zhu, M.B. Sun, Z.G. Wang, Experiments on flame stabilization in a scramjet combustor with a rear-wall-expansion cavity, Int. J. Hydrog. Energy 42 (2017) 26752–26761.
[11] J.C. Turner, M.K. Smart, Mode change characteristics of a three-dimensional scramjet at Mach 8, J. Propuls. Power 29 (2013) 982–990.
[12] Y. Zhang, B. Chen, G. Liu, B. Wei, X. Xu, Influencing factors on the mode transition in a dual-mode scramjet, Acta Astronaut. 103 (2014) 1–15.
[13] W. Shen, Y. Huang, Y.C. You, L. Yi, Characteristics of reaction zone in a dual-mode scramjet combustor during mode transitions, Aerosp. Sci. Technol. 99 (2020) 105779.
[14] R.F. Cao, Research on Combustion Mode Transition and Its Control Method for Scramjet Engines, Harbin Institute of Technology, 2016.
[15] M.L. Fotia, Mechanics of combustion mode transition in a direct-connect ramjet–scramjet experiment, J. Propuls. Power 31 (2015) 1–10.
[16] R. Cao, Y. Lu, D. Yu, J. Chang, Study on influencing factors of combustion mode transition boundary for a scramjet engine based on one-dimensional model, Aerosp. Sci. Technol. 96 (2020) 105590.
[17] C.L. Zhang, J.T. Chang, J.L. Zhang, W. Bao, D.R. Yu, Effect of continuous Mach number variation of incoming flow on ram-scram transition in a dual-mode combustor, Aerosp. Sci. Technol. 76 (2018) 433–441.
[18] B. An, Z. Wang, M. Sun, Ignition dynamics and combustion mode transitions in a rocket-based combined cycle combustor operating in the ramjet/scramjet mode, Aerosp. Sci. Technol. 118 (2021) 106951.
[19] C.L. Zhang, J.T. Chang, Y.S. Zhang, Y.Y. Wang, W. Bao, Flow field characteristics analysis and combustion modes classification for a strut/cavity dual-mode combustor, Acta Astronaut. 137 (2017) 44–51.
[20] K. Cabell, N. Hass, A. Storch, M. Gruber, HIFiRE direct-connect rig (HDCR) phase I scramjet test results from the NASA langley arc-heated scramjet test facility, in: 17th AIAA International Space Planes and Hypersonic Systems and Technologies Conference, 2011, pp. 2011–2248.
[21] B.G. Xiao, T. Ye, J.W. Xing, X.Y. Wang, Experimental and numerical investigations of combustion mode transition in a direct-connect scramjet combustor, Aerosp. Sci. Technol. 46 (2015) 331–338.
[22] Y. Tian, S.H. Yang, J.L. Le, T. Su, M. Yue, F. Zhong, X. Tian, Investigation of combustion and flame stabilization modes in a hydrogen fueled scramjet combustor, Int. J. Hydrog. Energy 41 (2016) 19218–19230.
[23] R. Masumoto, S. Tomioka, K. Kudo, A. Murakami, K. Kato, H. Yamasaki, Experimental study on combustion modes in a supersonic combustor, J. Propuls. Power 27 (2011) 346–355.
[24] W. Huang, Z.B. Du, L. Yan, R. Moradi, Flame propagation and stabilization in dual-mode scramjet combustors: a survey, Prog. Aerosp. Sci. 101 (2018) 13–30.
[25] T. Kouchi, G. Masuya, T. Mitani, S. Tomioka, Mechanism and control of combustion-mode transition in a scramjet engine, J. Propuls. Power 28 (2012) 106–112.
[26] R.F. Cao, J.T. Chang, B. Wen, M.L. Guo, Q. Jiang, D. Yu, Z. Wang, Analysis of combustion mode and operating route for hydrogen fueled scramjet engine, Int. J. Hydrog. Energy 38 (2013) 5928–5935.
[27] R.F. Cao, J.T. Chang, J.F. Tang, Z.Q. Wang, D.R. Yu, Study on combustion mode transition of hydrogen fueled dual-mode scramjet engine based on thermodynamic cycle analysis, Int. J. Hydrog. Energy 39 (2014) 21251–21258.
[28] Q. Yang, J. Chang, W. Bao, J. Deng, A mechanism of combustion mode transition for hydrogen fueled scramjet, Int. J. Hydrog. Energy 39 (2014) 9791–9797.
[29] X. Zhang, L.J. Yue, T.L. Huang, Q. Zhang, X. Zhang, Numerical investigation of mode transition and hysteresis in a cavity-based dual-mode scramjet combustor, Aerosp. Sci. Technol. 94 (2019) 105420.
[30] Y. Meng, H.B. Gu, J.H. Zhuang, W.M. Sun, Z. Gao, H. Lian, L. Yue, X. Chang, Experimental study of mode transition characteristics of a cavity-based scramjet combustor during acceleration, Aerosp. Sci. Technol. 93 (2019) 105316.
[31] H. Wang, N. Qin, M. Sun, H. Wu, Z. Wang, A hybrid LES (large Eddy simulation)/assumed sub-grid PDF (probability density function) model for supersonic turbulent combustion, Sci. China, Technol. Sci. 54 (2011) 2694.
[32] G.W. Ma, M.B. Sun, F. Li, Y.X. Yang, H.B. Wang, Effect of fuel injection distance and cavity depth on the mixing and combustion characteristics of a scramjet combustor with a rear-wall-expansion cavity, Acta Astronaut. 182 (2021) 432–445.
[33] F.R. Menter, Improved two-equation k-omega turbulence models for aerodynamic flows, Nasa Technical Memorandum, 1992.
[34] H.B. Wang, Z.G. Wang, M.B. Sun, N. Qin, Numerical study on supersonic mixing and combustion with hydrogen injection upstream of a cavity flameholder, Heat Mass Transf. 50 (2014) 211–223.
[35] G.Y. Zhao, M.B. Sun, H.B. Wang, H. Ouyang, Investigation of combustion characteristics in a scramjet combustor using a modified flamelet model, Acta Astronaut. 148 (2018) 32–40.
[36] G.Y. Zhao, J.H. Du, M.J. Liu, H.B. Wang, M.B. Sun, Numerical investigation of the scale effects of the flame flashback phenomenon in scramjet combustors, Aerosp. Sci. Technol. 119 (2021) 107165.
[37] G.Y. Zhao, J.H. Du, H.X. Yang, T. Tang, M.B. Sun, Effects of injection on flame flashback in supersonic crossflow, Aerosp. Sci. Technol. 120 (2022) 107226.
[38] G.Y. Zhao, M.B. Sun, J.S. Wu, H.B. Wang, A flamelet model for supersonic non-premixed combustion with pressure variation, Mod. Phys. Lett. B 29 (2015) 1550117.
[39] K. Narayanaswamy, H. Pitsch, P. Pepiot, A chemical mechanism for low to high temperature oxidation of n-dodecane as a component of transportation fuel surrogates, Combust. Flame 162 (2015) 1193–1213.
[40] H. Pitsch, http://www.stanford.edu/group/pitsch/FlameMaster.htm, 2008.
[41] N. Peters, Laminar diffusion flamelet models in non-premixed turbulent combustion, Prog. Energy Combust. Sci. 10 (1984) 319–339.
[42] L. Hou, D. Niu, Z. Ren, Partially premixed flamelet modeling in a hydrogen-fueled supersonic combustor, Int. J. Hydrog. Energy 39 (2014) 9497–9504.
[43] G.Y. Zhao, On the Excitation of Flame Flashback and Flame Propagation Mechanism in Supersonic Flow, National University of Defense Technology, 2019.